Journal of Astronomical Telescopes, Instruments, and Systems

AstronomicalTelescopes.SPIEDigitalLibrary.org

Design study of an image slicer module for a multiobject spectrograph

Shinobu Ozaki
Toshihiro Tsuzuki
Yoshiyuki Obuchi
Bungo Ikenoue
Satoshi Miyazaki
Jason R. Fucik
Kevin A. Bundy
Maureen Savage

SPIE.

Shinobu Ozaki, Toshihiro Tsuzuki, Yoshiyuki Obuchi, Bungo Ikenoue, Satoshi Miyazaki, Jason R. Fucik, Kevin A. Bundy, Maureen Savage, "Design study of an image slicer module for a multiobject spectrograph," *J. Astron. Telesc. Instrum. Syst.* **5**(3), 035001 (2019), doi: 10.1117/1.JATIS.5.3.035001.

Journal of Astronomical Telescopes, Instruments, and Systems 5(3), 035001 (Jul–Sep 2019)

Design study of an image slicer module for a multiobject spectrograph

Shinobu Ozaki,[a,*] Toshihiro Tsuzuki,[a] Yoshiyuki Obuchi,[a] Bungo Ikenoue,[a] Satoshi Miyazaki,[a] Jason R. Fucik,[b] Kevin A. Bundy,[c] and Maureen Savage[c]
[a]National Astronomical Observatory of Japan, Tokyo, Japan
[b]California Institute of Technology, Caltech Optical Observatories, Pasadena, California, United States
[c]University of California, UCO/Lick Observatory, Santa Cruz, California, United States

Abstract. We investigate an image slicer module for an optical multiobject spectrograph, wide-field optical spectrograph (WFOS), which is one of the first-light instruments of the Thirty Meter Telescope (TMT). The image slicer divides the target image into three slices, thus providing a one-third narrower slit width. By positioning a suite of such modules at the telescope focal surface, multiobject spectroscopy with high spectral resolution can be achieved. Three optical designs are developed: a two-mirror design, a four-mirror design, and a flat-mirror design. Comparing them, the flat-mirror design is found to be the most preferable for WFOS. From a tolerance analysis, the tolerances of manufacturing and assembling appear challenging but not insurmountable. We describe how the steep field curvature of TMT requires at least nine module variants, tuned to reduce defocus in specific focal surface zones. Finally, we introduce a viable mechanical packaging concept. [DOI: 10.1117/1.JATIS.5.3.035001]

Keywords: image slicer; multiobject spectroscopy; wide field optical spectrograph; thirty meter telescope.

Paper 19010 received Jan. 18, 2019; accepted for publication May 8, 2019; published online Jun. 6, 2019.

1 Introduction

Telescope apertures continue to increase because of our desire to observe fainter and more distant objects. As the telescope size increases, the physical scale of seeing-limited instruments increases in proportion. Extreme cases include instruments for the so-called "Extremely Large Telescopes," such as the Thirty Meter Telescope (TMT).[1] Corresponding instruments require huge optics, imposing technical challenges in manufacturing and supporting them. A specific example is the wide-field optical spectrograph (WFOS),[2–5] one of the TMT first-light instruments. It is being developed by an international collaboration led by the University of California Observatories. WFOS covers the wavelength range of 310 to 1000 nm and offers spectral resolving powers (R) of ~5000 and ~1000 in high and low dispersion modes, respectively.

To simultaneously cover the entire wavelength range even in the high dispersion mode, WFOS explored designs that utilized consecutive spectral orders obtained from cross-dispersion prisms in addition to the main reflective gratings. This approach was used in the multiobject Echellette mode[6] for IMACS[7] on the Magellan Telescope. However, it was found that, even with camera systems whose largest lens diameter was ~440 mm, vignetting was ~40% at the field edge. This diameter of 440 mm represents the largest size of currently available calcium fluoride blanks. Therefore, enlarging the camera diameter further was considered very high risk.

The vignetting can be reduced using a transmission disperser because the camera systems can be located closer to the dispersers at an internal pupil location. A transmission volume phase holographic (VPH) grating is broadly used for astronomical instruments because of its high efficiency. However, since it works only in the first spectral order, the entire wavelength range cannot be simultaneously covered in the high dispersion mode. In the case of a grism, the prism apex angle is required to be >66 deg to get $R = 5000$ for affordable materials. Considering the internal pupil diameter of 300 mm, such a grism would be prohibitively large and does not enable us to put the camera systems close to the pupil. In the case of a transmission blazed grating, to get $R \sim 5000$ the incident angle is ~43 deg. For such a large incident angle, the refractive index (n) needs to be >2.2. However, materials with $n > 2.2$ are limited to special ones such as diamond or ZnSe, with no affordable alternatives. There is a development effort underway for a new transmission grating achieving $R = 5000$ with an affordable material, but it is still under development.[8]

Facing this situation, the WFOS development team decided to study alternate concepts.[5,9] Slicer-WFOS is one of these concepts. It uses a series of image slicers to achieve higher spectral dispersion while maintaining target multiplex. An image slicer has been used for high dispersion spectrographs such as high dispersion spectrograph[10] on the Subaru telescope and UV-visual high-resolution Echelle spectrograph[11] on Very Large Telescope (VLT). Those instruments adopt the Bowen–Walraven type slicer[12,13] or a variation. However, these designs are optimized for point-like objects and hence are not proper for extended objects such as galaxies. For extended objects, a longer pseudoslit is required. One example is the image slicer of X-shooter[14] on VLT that has the pseudoslit length of 4 arc sec, although it is a single-object spectrograph. Slicer-WFOS is required to be capable of multiobject spectroscopy.

In this paper, we report our conceptual study of the image slicer for Slicer-WFOS. After explaining the Slicer-WFOS concept in Sec. 2, three optical designs are introduced and compared in Sec. 3. In Sec. 4, a technical challenge imposed by the TMT

*Address all correspondence to Shinobu Ozaki, E-mail: shinobu.ozaki@nao.ac.jp

2329-4124/2019/$28.00 © 2019 SPIE

field curvature is described. In Sec. 5, we briefly describe considerations on reflection coatings. Finally, conceptual mechanical structures of the slicer module and the exchange system are shown in Sec. 6.

2 Slicer-WFOS Concept

The primary instrument parameters of Slicer-WFOS are summarized in Table 1. In this concept, transmission VPH gratings are used for both the red and blue arms (Fig. 1). The gratings offer $R \sim 1500$ for a 0.75-arc sec-width slit and cover the entire wavelength range in one exposure. In the high dispersion mode, small image slicer modules are positioned on the telescope focal surface instead of a slit mask. The image slicer divides a 0.75-arc sec-aperture width into three slices with the width of 0.25 arc sec each, and the higher spectral resolution of $R \sim 4500$ can be achieved using the same grating as in the low dispersion mode. The pixel scale of Slicer-WFOS is ~0.05 arc sec /pixel, assuming the pixel size of 15 μm, and hence the slice width is sampled by ~5 pixels.

Simply using a narrow slit with 0.25-arc sec width, $R \sim 4500$ can be achieved. However, in this case, only about 33% of light from a point source can be captured under 0.7 arc sec seeing (Fig. 2). When reflectivity of 98% is assumed for each mirror of the slicer module (see Sec. 5), the throughput is not largely degraded from the 0.75-arc sec-slit case, and the fraction of light entering WFOS is ~75%. In addition, it should be noted that, even in the high dispersion mode, the entire wavelength range can also be covered in one exposure. The transmission VPH grating allows us to locate the cameras closer to the input pupils. In addition, the input pupils maintain a circular shape with a 300-mm diameter because the gratings are used in the Littrow configuration. These features make the camera optical design easier and the vignetting lower.

Table 1 Instrument parameters of Slicer-WFOS.

Field of view	8.3 arc min × 3 arc min
Spectral resolution	$R = 1500$ and 4500 for 0.75-arc sec-slit width
Wavelength coverage	310 to 1000 nm
Collimator focal length	4500 mm
Camera focal length	600 mm

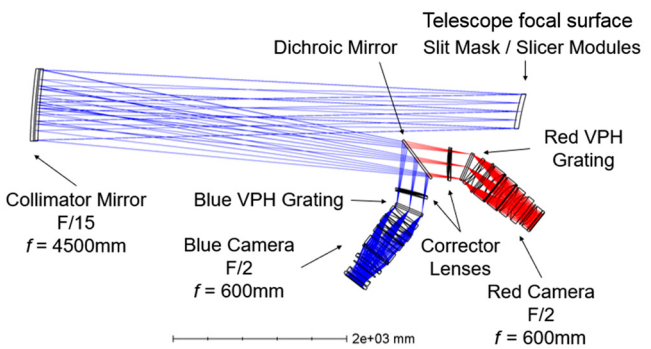

Fig. 1 Optical layout of Slicer-WFOS.

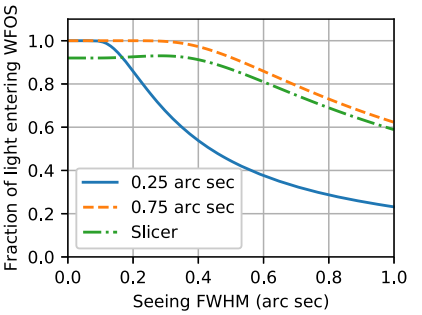

Fig. 2 Fraction of light entering WFOS for 0.25-arc sec- and 0.75-arc sec-slit widths and the slicer. A point source with the Gaussian radial profile is assumed. In the slicer case, estimated throughput of the slicer module is taken into account (see Sec. 5).

3 Optical Design of the Image Slicer

3.1 *Requirements*

The basic requirements for the image slicer are summarized in Table 2. The slice width is 550 μm, corresponding to 0.25 arc sec on sky. The slice length is 15.3 mm, corresponding to 7 arc sec on sky, which is required for precise sky subtraction using a nodding method. Considering the total slit length of 8.3 arc sec, the maximum multiplicity is 23 including some margin for opto-mechanics. A requirement for the output beam direction deviation with respect to the original direction must be considered. TMT does not have adequate baffles, and therefore WFOS will have an internal baffle in order to reduce stray light. The baffle is located at the internal pupil image. If the output beam direction significantly deviates from that of the input beam, the pupil image shifts significantly. This causes larger vignetting at the baffle and increases stray light. We therefore require less than 0.115 deg angular deviations, corresponding to a 3% pupil shift.

3.2 *Two-Mirror Design*

To coexist with the low dispersion mode using a simple slit mask, the slicer module is required to provide an exit pupil and exit F ratio identical to those of the telescope, and the pseudoslits are also required to be at the telescope focal surface. Since those requirements can be satisfied with at least two surfaces, our initial design was the two-mirror system. The slice mirrors are at the telescope focal surface and do not change the F ratio. When the recreated image by the second mirror is located on the telescope focal surface, the curvature radius (R_{2nd}) of the second mirror must be equal to the distance (d) between the slice mirror and the second mirror [Fig. 3(a)]:

$$R_{2nd} = d.$$

Table 2 Basic requirements for the image slicer.

Slice width	550 μm (0.25 arc sec)
Slice length	15.3 mm (7 arc sec)
Slice number	3
Output beam direction deviation	<0.115 deg

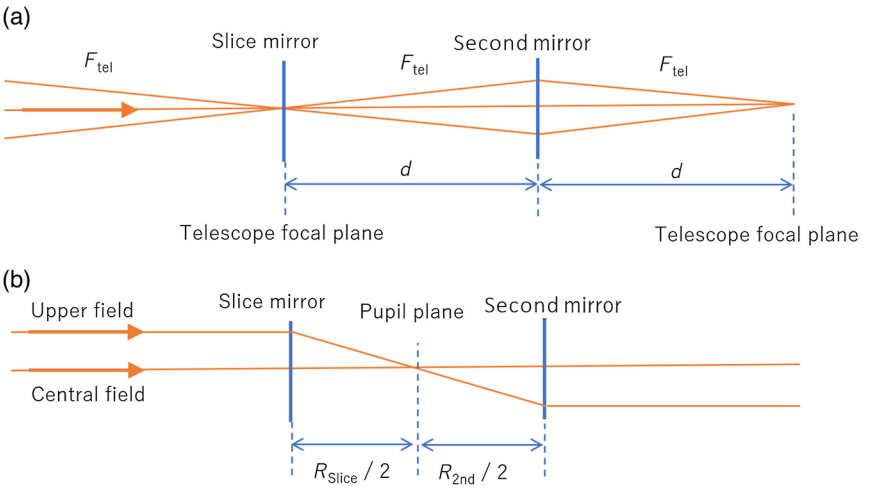

Fig. 3 Geometrical concept of the two-mirror design. For illustration purposes, all mirrors are described as transmission optics. (a) Light rays only for the central field of a slice mirror are shown. (b) Only chief rays for the central and upper fields of a slice mirror are shown.

When the input beam from the telescope is assumed to be telecentric, the pupil image is created at $R_{\mathrm{slice}}/2$ from the slice mirror [Fig. 3(b)], where R_{slice} is the curvature radius of the slice mirror. Because the output beam from the second mirror must be also telecentric, the second mirror must be located at $R_{2\mathrm{nd}}/2$ from the pupil image, and then

$$\frac{R_{\mathrm{slice}}}{2}+\frac{R_{2\mathrm{nd}}}{2}=d.$$

Considering $R_{2\mathrm{nd}}=d$

$$R_{\mathrm{slice}}=R_{2\mathrm{nd}}=d.$$

Hence, there is only one free parameter in the two-mirror design.

Figure 4 shows the optical design. All mirrors have concave spherical surfaces with an identical curvature radius. For the central slice, there is no slice mirror and incoming light passes through the module. Incoming light to the two side slices is reflected by the slice mirrors and reimaged next to the center slice on the telescope focal surface by the secondary mirrors. For ease of manufacturing, the actual slice mirrors have larger size than the reflection area and are masked for unused area (Fig. 5).

This design shows sufficiently good image quality in comparison with the pseudoslit width of 550 μm (Fig. 6), although optimization was not thoroughly applied. However, we found

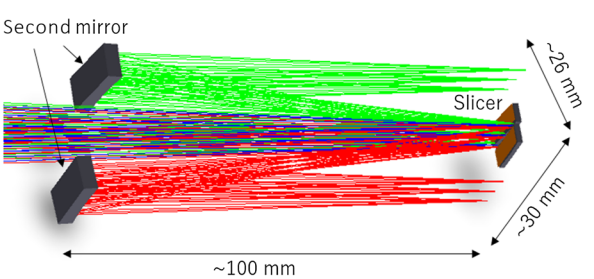

Fig. 4 Optical layout of the two-mirror design. Light from the telescope comes from the left. Blue rays are for the central slice. Green and red ones are for the two side slices.

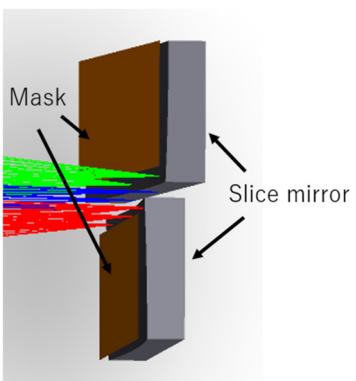

Fig. 5 Magnified view of the slice mirrors. Larger mirrors are masked except the reflection area.

large module-tilt sensitivity of the output beam direction. The output beam tilts by about twice the module tilt. For example, when the module tilts by 0.5 deg, the output beam tilts by about 1 deg with respect to the original direction. This can be easily

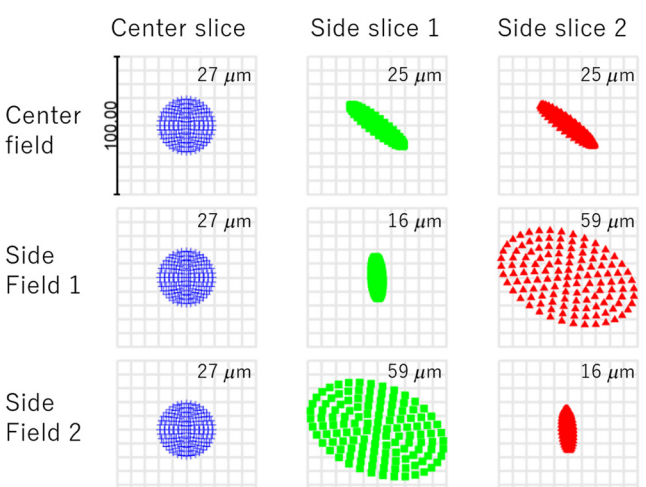

Fig. 6 Spot diagram of the two-mirror design. The box size is 100 μm. RMS diameters are shown at the top right corner of each panel.

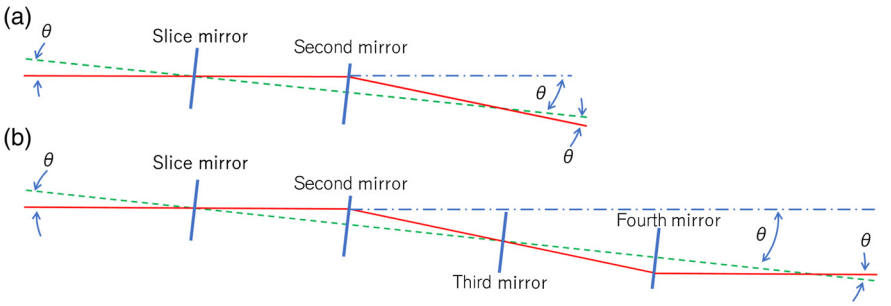

Fig. 7 Geometrical interpretation of the module-tilt sensitivity of (a) the two-mirror design and (b) the four-mirror design. Green dashed lines are the optical axis of the module. Red solid lines show the chief rays after tilting the module.

interpreted as a natural feature of the second mirror with an equal magnification [Fig. 7(a)]. When the module is tilted by θ, the output beam chief ray is also tilted by θ with respect to the optical axis of the module because the distance between the slicer and the second mirror is the same as the distance between the second mirror and the recreated image. Since the axis is also tilted by θ to the same direction, the angle between the output beam chief ray and the input beam chief ray is 2θ.

3.3 *Four-Mirror Design*

When an identical mirror pair [third and fourth mirrors in Fig. 7(b)] is added after the second mirror, the tilt sensitivity can be canceled. In this case, the output chief ray is also tilted by θ with respect to the module axis, but its rotation direction is opposite to the angle from the input chief ray to the module axis. This is the four-mirror concept described further in this section.

Figure 8 shows the optical layout of the four-mirror design. Similar to the two-mirror design, all mirrors have concave spherical surfaces with an identical curvature radius. In this design, the module-tilt sensitivity of the output beam direction is dramatically improved. For the module tilt of 0.5 deg, the output beam tilts only by ~0.05 deg with respect to the original direction. The spot RMS diameters are <50 μm at the telescope focal surface, which is well below the pseudoslit width of 550 μm (Fig. 9).

Figure 10 shows the tolerance analysis result for the output beam direction using a Monte Carlo approach. In this analysis, tilt and decenter amplitudes of each mirror are assumed to be within 0.02 deg and 30 μm, respectively. We found that this design met requirements on the output beam deviation about 52% of the time. This is because tilt errors and the decenter of each mirror act to degrade the performance, although the module tilt is almost insensitive to the output beam direction error. To improve on this, higher manufacturing and assembling accuracies are needed but were deemed challenging.

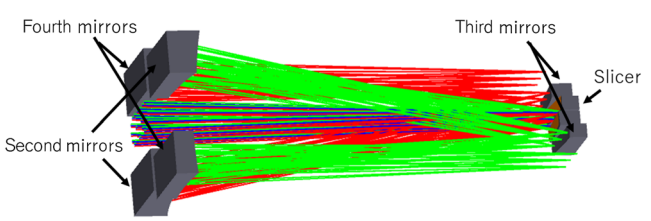

Fig. 8 Optical layout of the four-mirror design. Light from the telescope comes from the left. Blue rays are for the central slice. Green and red show those of the two side slices.

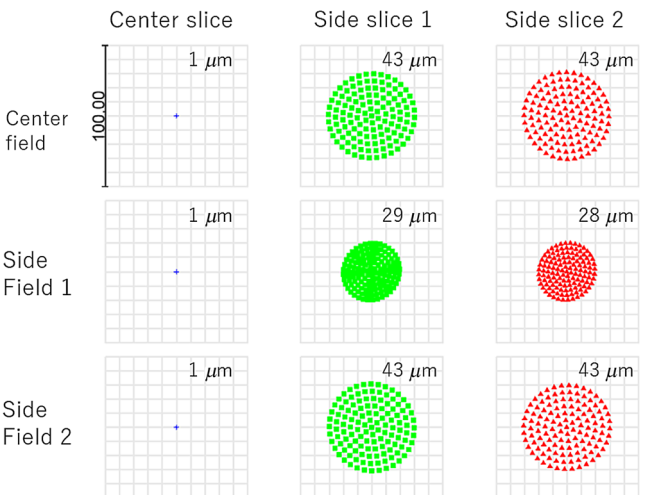

Fig. 9 Spot diagram of the four-mirror design. The box size is 100 μm. RMS diameters are shown at the top right corner of each panel.

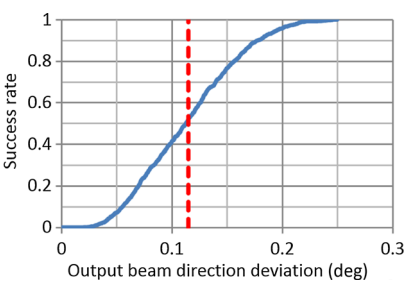

Fig. 10 Tolerance analysis result for the four-mirror design. Red dashed line shows the requirement (0.115 deg).

3.4 *Flat-Mirror Design*

To meet the specification for the output beam direction deviation, a completely new design was introduced (Fig. 11). In this design, all mirrors are flat. Hence, there is no image quality degradation. Incoming light for the two side slices is reflected by the slice mirrors and reflected again by the secondary mirror. Viewed from the spectrograph, the virtual pseudoslit images are located behind the secondary mirrors. Incoming light for the central slice passes through the image slicer and goes through four mirrors to match the virtual pseudoslit location to the other two. The pseudoslit configuration at the virtual image surface is shown in Fig. 12. The total pseudoslit length is 47 mm including gaps between the spectra.

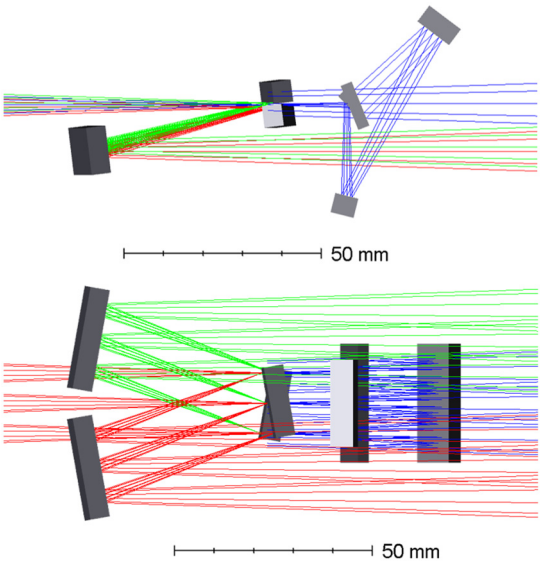

Fig. 11 Optical design of the flat-mirror design. Light from the telescope comes in from the left. Blue rays show the light of the central slice. Green and red rays show the light of the two side slices.

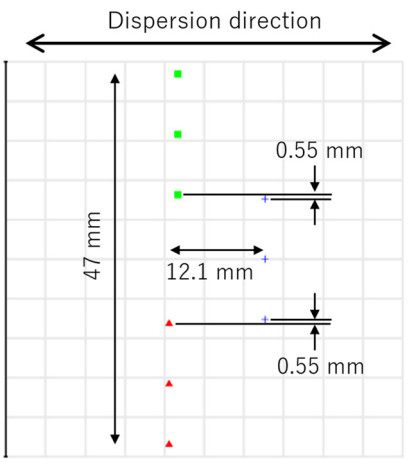

Fig. 12 Relative position of three pseudoslits on the virtual image surface. Center and two edge points of each pseudoslit are shown. Each pseudoslit length is ~15.3 mm. Gaps between spectra are ~0.55 mm. The central pseudoslit is shifted by ~12.1 mm along the dispersion direction. The grid step is 5 mm.

An optical system consisting of an even number of flat mirrors shows no module-tilt sensitivity of the output beam direction. In addition, the decenter of each mirror does not affect the reflection direction. Therefore, we can expect better performance regarding the output beam direction deviation. For the central channel, the first and the fourth mirrors are located at the front and the rear surfaces of a wedged glass plate so that assembly error of this wedged plate is canceled out. According to the tolerance analysis with the parameter ranges identical to those in Fig. 10, the requirement on the output beam direction deviation is achieved nearly 100% of the time (Fig. 13).

In Slicer-WFOS as with other imaging spectrographs, the collimator's conjugate focal surface is matched to the telescope focal surface. The slicer modules are installed in the spectrograph so that the virtual pseudoslits locate at the collimator's

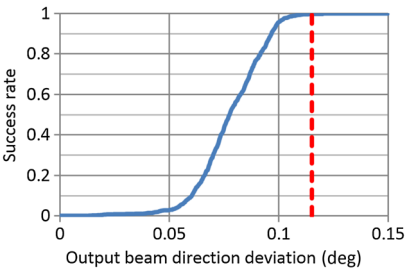

Fig. 13 Tolerance analysis result for the flat-mirror design. Red dashed line shows the requirement (0.115 deg).

conjugate focal surface. To do so, the image slicers must be placed ~100 mm away from the nominal telescope focus. Hence, in the high dispersion mode, the telescope secondary mirror is shifted slightly to align the telescope focal surface with the slicers. We confirmed that this secondary mirror shift does not significantly degrade image quality.

3.5 *Design Comparison*

A comparison of the three designs described above is summarized in Table 3. All designs show sufficiently good image quality for a pseudoslit width of 550 μm, with the flat-mirror design showing no appreciable image quality degradation. The two-mirror design exhibits large module-tilt sensitivity in the output beam deviation, which we deem unacceptable. The four-mirror design has a much smaller sensitivity. However, when manufacturing and assembling errors are considered, the expected success rate in meeting requirements is only 52%. The flat-mirror design has negligible module-tilt sensitivity and is expected to meet our specifications, even when manufacturing and assembling errors are taken into consideration. In addition, its manufacturability is most straightforward among the designs considered because all mirror surfaces are flat, although the number of mirrors is obviously greater than that of the two-mirror design. Although the telescope secondary mirror must be slightly shifted, image quality can be preserved. Considering its excellent performances, we conclude that the flat-mirror design is preferable for Slicer-WFOS.

Table 3 Design comparison.

	Two-mirror	Four-mirror	Flat-mirror
Image quality (RMS diameter)[a]	59 μm[b]	43 μm	0 μm
Success rate for the output beam direction deviation	–[c]	52%	100%
Telescope secondary mirror shift	Not required	Not required	Required
Number of mirrors	4	8	8
Surface figure of mirrors	Sphere	Sphere	Flat

[a]Image quality of the image slicer.
[b]Optimization was not thoroughly applied.
[c]The Monte Carlo analysis was not performed.

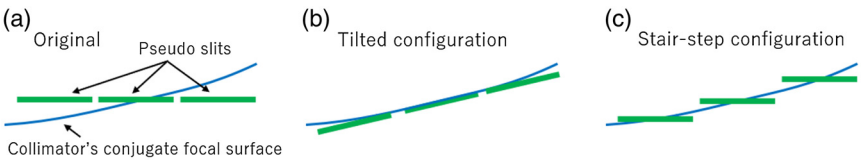

Fig. 14 Pseudoslit configurations. Three green lines exhibit pseudoslits and the blue curved line shows the collimator's conjugate focal surface at the outer region in the Slicer-WFOS field.

4 Adaptation for the TMT Field Curvature

TMT has a steep field curvature with a radius of ∼3 m and the collimator matches this field curvature. Considering the total length of the three pseudoslits (47 mm), if the three pseudoslits are located on an identical plane perpendicular to the telescope optical axis, the pseudoslit edges of the two side slices will be out of defocus with respect to the collimator in the outer WFOS field [Fig. 14(a)]. To reduce this defocus, two variations of the pseudoslit configurations were studied: a tilted configuration and a stair-step configuration [Figs. 14(b) and 14(c)]. In the tilted configuration, the slicer is tilted to align with the local slope of the telescope focal surface. As a result, the virtual pseudoslits also align with the local slope of the collimator's conjugate focal surface. In the stair-step configuration, the pseudoslits locations are matched to the collimator's conjugate focal surface by changing the mirror positions. Each pseudoslit does not tilt in this case.

These configurations require different kinds of designs for different field positions. In the tilted configuration, we found that at least nine kinds of designs are required to cover the entire Slicer-WFOS field (Fig. 15). Figure 16 shows one example having a 9-deg tilt angle. The central pseudoslit is slightly offset along the telescope optical axis with respect to the two side pseudoslits. This enables it to trace the field curvature along the dispersion direction. In the stair-step configuration, the required number of the design variants was significantly greater. Therefore, we did not pursue the stair-step configuration.

It was found that three or four modules are required for each design to cover each field region. As a result, to cover the entire field, at least 29 modules must be prepared in total. This number (29) is not equal to the maximum multiplicity (23). The slicer field-of-view exists around the central pseudoslit on the projected plane shown in Fig. 17. For example, when an object is at a position immediately to the left of the border of two regions covered by designs A and B (right inset of Fig. 17), we have to use design A. On the other hand, when an object is to the right of the border, we have to use design B. The number of modules simultaneously used is less than or equal to the maximum multiplicity.

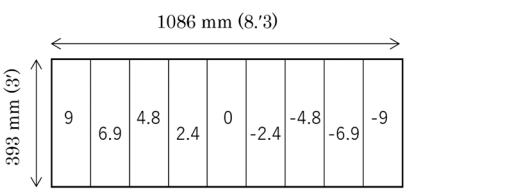

Fig. 15. Regions covered by nine kinds of designs in the Slicer-WFOS field of 1086 × 393 mm on the telescope focal surface. Numbers denoted in the each region show the tilt angles in the designs. The dispersion direction is vertical in this figure.

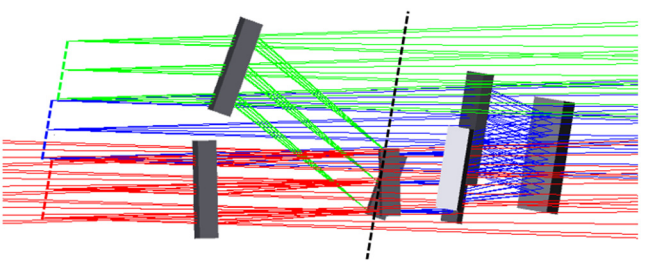

Fig. 16 Tilted design example. The black dashed line shows the tilt angle of the slicer. Colored dashed lines show the virtual pseudoslits.

5 Coating

In the optical range, aluminum and silver are frequently used for reflective coatings. Aluminum coatings have a dip in reflectivity around 850 nm to ∼85%. Even for wavelengths outside of this dip, the reflectivity is ∼92%. Considering the four mirrors for the central slice, the throughput due to aluminum reflection losses will decrease to ∼52% at the dip and ∼72% outside the dip. When a dielectric coatings are added on top of aluminum to enhance the reflectivity at the dip, it is commonly found

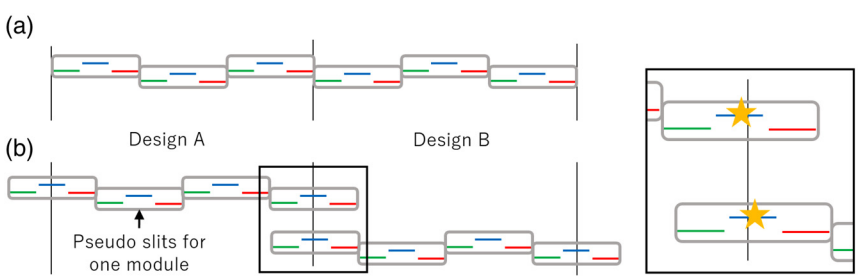

Fig. 17 For illustration purposes, two field regions covered by designs A and B are considered. Each region has a width equivalent to three total-pseudoslit-length widths. In this case, (a) the multiplicity is six. However, in order to obtain data for a target close to the border, we need more modules, as shown in (b) (eight in this case). The right inset is the magnified view around the border. Object positions for the two modules are shown by stars.

that the reflectivity at 310 nm, the blue limit for Slicer-WFOS, decreases significantly.

Reflectivity of silver rapidly drops from 400 nm to shorter wavelengths. UV-enhanced silver coating developed for the Gemini telescopes has high reflectivity even at wavelengths shorter than 400 nm.[15] However, it shows very low reflectivity at 310 nm.

One solution is a high reflectivity coating using only multilayer dielectric coating. According to a coating vendor we inquired with, reflectivity greater than 98% over 310 to 1000 nm is achievable in theory. They noted that, in the actual products, there might be sharp dips in reflectivity at some wavelengths due to manufacturing error. If the reflectivity is more than 98%, the combined throughput is ~92% and ~96% for the central and side slices, respectively.

6 Mechanical Concept

6.1 *Slicer Module*

Figure 18 shows a conceptual design for the mechanical structure of the slicer module. The orange part holds two slice mirrors and two second mirrors for the two-side channels. The gray part holds four mirrors for the central channel. Each part is monolithically fabricated. There is no alignment-adjusting mechanism for all mirrors. All mirrors are held in place with clips to press reference surfaces in the mechanical structure. They are not bonded to the mechanical structure in order to avoid stress due to temperature changes between assembling and observation. Slicer-WFOS is envisioned to have an enclosure in which the temperature is controlled at $0 \pm 0.1^{\circ}$C. Hence, temperature changes during observations are not a concern.

The reference surfaces must be fabricated with sufficient precision. From a tolerance analysis, we found that μm-level fabrication accuracy is required. A high precision five-axis machining center would be able to achieve this accuracy even for this complex structure. Tilt error in assembling the two parts does not contribute to output beam deviations because the mirrors for each channel are held by either part and because the flat-mirror design does not show appreciable module-tilt sensitivity (see Sec. 3.4).

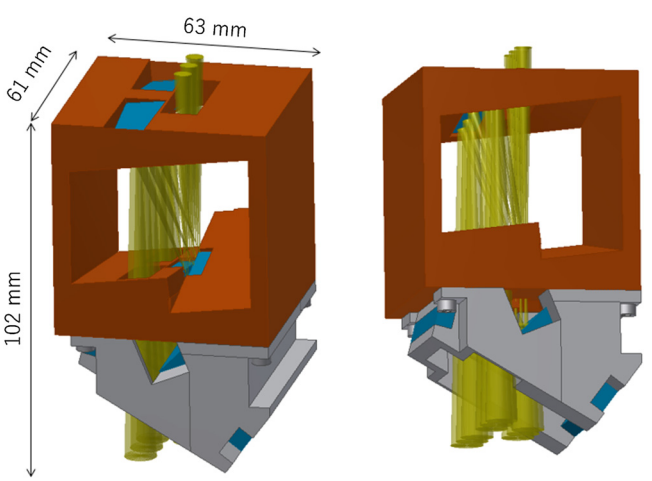

Fig. 18 Conceptual mechanical structure of the slicer module. It consists of two parts (orange and gray parts). Light and the mirrors are shown by yellow and blue, respectively.

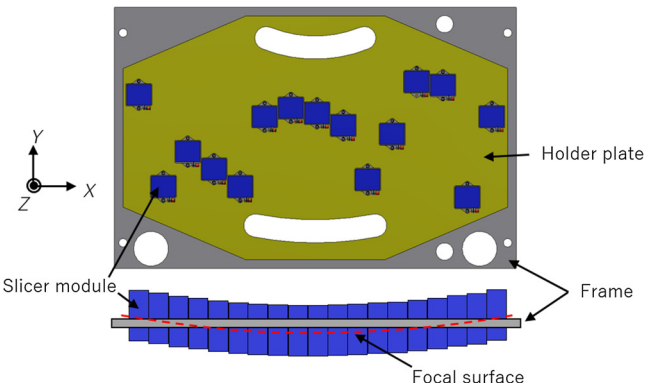

Fig. 19 Mask plate for the slicer modules. It consists of a frame (gray) and a holder plate (yellow). The slicer modules (blue) are clamped with clamp mechanisms shown in Fig. 21. Red dashed line is the telescope focal surface. Two arc-like apertures at the top and bottom of the holder plate are the patrol areas for two guiding cameras.

6.2 *Mask Plate for the Slicer Modules*

A mask plate for the slicer modules consists of a frame and a holder plate (Fig. 19). The slicer modules are plugged into a mask plate so that the slice mirrors of each module are located at the telescope focal surface using a template surface (Fig. 20) and then clamped (Fig. 21). The holder plate is discarded after the observation, but the frame is reused.

Position errors of the slicer module were estimated from a root square sum of putative error contributions assuming manufacturing errors (flatness of 0.02 mm, location error of 0.05 mm, and angular error of 0.05 deg) and the fitting tolerance of 0.05 mm. Estimated errors are summarized in Table 4. These positioning errors cause a displacement of the slice mirror with respect to an object image. Assuming the rotation center is

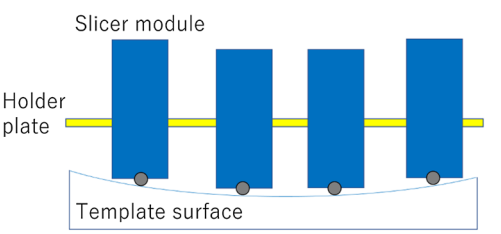

Fig. 20 Template surface to define the slicer module depth.

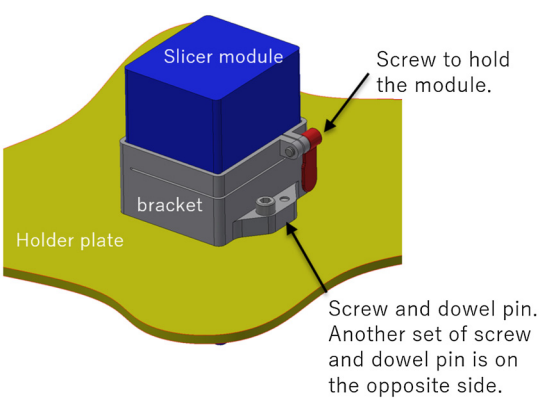

Fig. 21 Clamp mechanism to clamp the slicer module to the folder plate.

Table 4 Position error of the slicer module. Axis directions are shown in Fig. 19.

	Estimated errors
X (mm)	0.066
Y (mm)	0.066
Z (mm)	0.114
θ_X (deg)	0.075
θ_Y (deg)	0.078
θ_Z (deg)	0.217

at the holder plate, the slice mirror displacement is estimated to be ~0.2 mm at most. This causes 2% to 3% light loss for 0.7-arc sec seeing.

6.3 *Exchange Mechanism*

An exchange mechanism has not been studied in depth because the WFOS mechanical structure is not yet clearly defined. Figure 22 shows one of the possible concepts. A robotic arm next to WFOS assembles the mask plate for the slicer modules; it puts the holder plate on the frame and plugs the slicer modules into the holder plate. After an exposure, the WFOS rotating structure is rotated to a certain position, and the old mask plate is slid out using rails embedded in the WFOS rotating structure. The robotic arm exchanges the previous plate with the newly plugged one. During the exposure, the robotic arm disassembles the old mask plate and assembles a new mask plate for the next observation.

7 Summary

We have studied image slicer modules that enable a high spectral dispersion mode for the multiobject spectrograph, WFOS. Three optical designs of the slicer module have been developed and compared. We found that the module-tilt sensitivity to the output beam deviation imposes tight tolerances. A two-mirror design shows the unacceptable sensitivity. A four-mirror design dramatically reduces the sensitivity, but the tolerances of manufacturing and assembling are too tight. A flat-mirror design shows no module-tilt sensitivity. Although the tolerances are looser than the other two, they are still challenging. We suggest that a five-axis high precision machining center would achieve the μm-level fabrication accuracy required for the slicer module structure. We concluded that the flat-mirror design is the most preferable for Slicer-WFOS.

We also found that, to adapt the TMT field curvature, the slicer must be aligned to the local slope of the telescope focal surface. This requires at least nine kinds of designs to cover the entire WFOS field and 29 modules in total.

Finally, we introduced mechanical concepts for the slicer module and exchange mechanism. The expected positioning error of the slicer module causes 2% to 3% light loss due to the lateral displacement of the slice mirror with respect to the object image.

The Slicer-WFOS concept has not been selected as a baseline because of its operational complexity and the technical challenge in manufacturing. As we describe, although μm-level accuracy is required for manufacturing the optomechanics, it can be achieved using a high precision five-axis machining center. TMT considered the associated risks for such a first-light instrument too great, especially in light of other design solutions for the WFOS instrument.

Acknowledgments

The authors would like to thank Bernard Delabre for providing the original idea of the flat-mirror design. We also appreciate the in-depth discussions with Noboru Ebizuka about dispersers. The TMT Project gratefully acknowledges the support of the TMT collaborating institutions. They are the California Institute of Technology, the University of California, the National Astronomical Observatory of Japan, the National Astronomical Observatories of China and their consortium partners, the Department of Science and Technology of India and their supported institutes, and the National Research Council of Canada. This work was supported as well by the Gordon and Betty Moore Foundation, the Canada Foundation for Innovation,

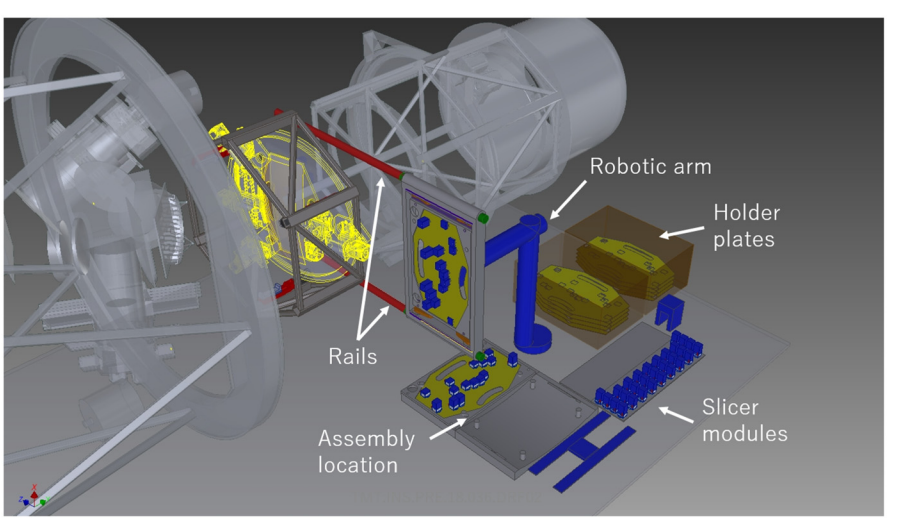

Fig. 22 Exchange mechanism concept.

the Ontario Ministry of Research and Innovation, the Natural Sciences and Engineering Research Council of Canada, the British Columbia Knowledge Development Fund, the Association of Canadian Universities for Research in Astronomy (ACURA), the Association of Universities for Research in Astronomy (AURA), the U.S. National Science Foundation, the National Institutes of Natural Sciences of Japan, and the Department of Atomic Energy of India.

References

1. G. H. Sanders, "The Thirty Meter Telescope (TMT): an international observatory," *J. Astrophys. Astron.* **34**, 81–86 (2013).
2. R. A. Bernstein and B. C. Bigelow, "An optical design for a wide-field optical spectrograph for TMT," *Proc. SPIE* **7014**, 70141G (2008).
3. B. C. Bigelow and R. A. Bernstein, "Progress of the conceptual design for the MOBIE imaging spectrograph for the Thirty Meter Telescope," *Proc. SPIE* **7735**, 773527 (2010).
4. B. C. Bigelow et al., "Conceptual design of the MOBIE imaging spectrograph for TMT," *Proc. SPIE* **9147**, 914728 (2014).
5. K. Bundy et al., "WFOS instrument trade study: slicer vs. fiber instrument concept designs and results (conference presentation)," *Proc. SPIE* **10702**, 1070220 (2018).
6. B. M. Sutin and A. McWilliam, "Multi-object high-resolution Echellette spectroscopy with IMACS," *Proc. SPIE* **4841**, 1357–1366 (2003).
7. A. Dressler et al., "IMACS: the Inamori–Magellan areal camera and spectrograph on Magellan–Baade," *Publ. Astron. Soc. Pac.* **123**, 288–332 (2011).
8. N. Ebizuka et al., "Novel diffraction gratings for next generation spectrographs with high spectral dispersion," *Proc. SPIE* **9912**, 99122Z (2016).
9. S. Ozaki et al., "Image slicer module for wide field optical spectrograph (WFOS)," *Proc. SPIE* **10702**, 107028M (2018).
10. A. Tajitsu, W. Aoki, and T. Yamamuro, "Image slicer for the Subaru telescope high dispersion spectrograph," *Publ. Astron. Soc. Jpn.* **64**, 77 (2012).
11. H. Dekker et al., "High S/N, high resolution image slicer observations with UVES," *Proc. SPIE* **4842**, 139–150 (2003).
12. I. S. Bowen, "The image-slicer, a device for reducing loss of light at slit of stellar spectrograph," *Astrophys. J.* **88**, 113–124 (1938).
13. T. Walraven and J. H. Walraven, "Some features of the Leiden radial velocity instrument," in *Auxiliary Instrumentation for Large Telescopes*, S. Laustsen and A. Reiz, Eds., pp. 175–183 (1972).
14. I. Guinouard et al., "An integral field unit for X-shooter," *Proc. SPIE* **6273**, 62733R (2006).
15. T. Schneider and P. Stupik, "A UV-enhanced protected silver coating for the Gemini telescopes," *Proc. SPIE* **10700**, 1070048 (2018).

Shinobu Ozaki is a specially appointed research staff member at the National Astronomical Observatory of Japan. He received his PhD in astronomy from Kyoto University in 2009. His current research interests include galaxy formation and active galactic nuclei. He has been working on developing integral field units for various telescopes and has been involved in WFOS since 2010.

Biographies of the other authors are not available.